NASA/TM—2002-211379

AIAA–2002–0542

Response Surface Modeling of Combined-Cycle Propulsion Components Using Computational Fluid Dynamics

C.J. Steffen, Jr.
Glenn Research Center, Cleveland, Ohio

Prepared for the
40th Aerospace Sciences Meeting and Exhibit
sponsored by the American Institute of Aeronautics and Astronautics
Reno, Nevada, January 14–17, 2002

National Aeronautics and
Space Administration

Glenn Research Center

March 2002

Acknowledgments

I would like to acknowledge the important role played by Mr. Dennis Keller (1955–2001) with regard to the work presented. He was a friend, teacher, and informed advocate for modern experiment design at NASA Glenn. His coursework on modern statistical analysis has contributed to dozens of improvements in experimental design for aerospace research at NASA Glenn. His contributions will be sorely missed.

This report contains preliminary findings, subject to revision as analysis proceeds.

Available from

NASA Center for Aerospace Information
7121 Standard Drive
Hanover, MD 21076

National Technical Information Service
5285 Port Royal Road
Springfield, VA 22100

Available electronically at http://gltrs.grc.nasa.gov/GLTRS

Response Surface Modeling of Combined-Cycle Propulsion Components Using Computational Fluid Dynamics

C.J. Steffen, Jr.
National Aeronautics and Space Administration
Glenn Research Center
Cleveland, Ohio 44135
E-mail: *c.j.steffen@grc.nasa.gov*

Abstract

Three examples of response surface modeling with CFD are presented for combined cycle propulsion components. The examples include a mixed-compression-inlet during hypersonic flight, a hydrogen-fueled scramjet combustor during hypersonic flight, and a ducted-rocket nozzle during all-rocket flight. Three different experimental strategies were examined, including full factorial, fractionated central-composite, and D-optimal with embedded Plackett-Burman designs. The response variables have been confined to integral data extracted from multidimensional CFD results. Careful attention to uncertainty assessment and modeling bias has been addressed. The importance of automating experimental setup and effectively communicating statistical results are emphasized.

1 Motivation

Combined-cycle propulsion (CCP) vehicles rely upon the promise of airbreathing-propulsion to improve the impulse efficiencies normally associated with conventional chemical-propulsion technologies. Both turbine-based and rocket-based combined cycles have received a great deal of attention within the past decade. Turbine-based combined cycle engines have the advantage of a very mature low-speed system technology. On the other hand, rocket-based combined-cycle engines tend to have a single flowpath used throughout the entire ascent trajectory for a single-stage-to-orbit (SSTO) design. An axisymmetric, four-mode RBCC propulsion technology program, known as GTX, has been studied at NASA for the last five years. Figure 1(a) shows a reference vehicle concept and Figure 1(b) shows the flowpath in cross-section.

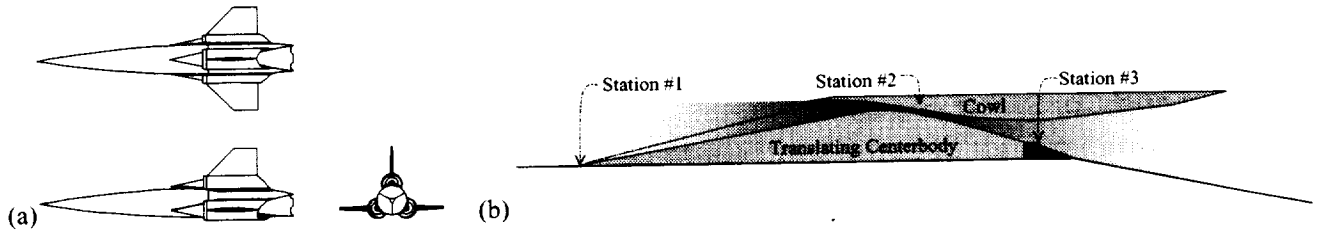

Figure 1 NASA RBCC concept: (a) GTX reference vehicle and (b) axi-symmetric engine flowpath geometry

Design simplicity is a key attribute of the GTX propulsion system, which consists of an axisymmetric engine design. Engine operation is defined by four separate modes during an ascent trajectory[1] from earth to orbit. First, the engine functions with the rocket ignited in a unique Ejector-Ramjet cycle[2] (mode 1), known as the independent ramjet stream (IRS) cycle. Then the rocket engine is switched off and subsonic combustion is present in the ramjet (mode 2). As the vehicle continues to accelerate, supersonic combustion occurs in the scramjet (mode 3). The rocket is eventually re-ignited (mode 4) for the final ascent into orbit in an all-rocket configuration. The single piece of moving hardware, throughout this ascent profile, is the translating centerbody of the inlet. Further details on this CCP design and reference vehicle concept are given by Trefny[3].

Four different propulsion cycles define a complex trade space. A workable system must optimize overall objectives, as a function of separate component performances. This design effort continually refines the GTX concept, based on ever-increasing fidelity in the performance analysis. This leads to an expanding level of definition in the GTX propulsion system design. The technology maturation phase of the GTX program is directed towards the assessment of sub-systems that cover a particular component and/or propulsion cycle. This approach assumes that when pieced together, a comprehensive systems-level trade study can be executed. An engineering approach of parametric experimentation and analysis has been employed to define sub-system performance over a broad range of operating conditions[4]. A combination of ground test experiments, computational fluid dynamic (CFD) simulations, and eventual flight test experiments have been employed to achieve this end. Statistical design of experiments (DOE) offers a particularly efficient way to conduct these numerous parametric studies.

2 CFD and Statistical Experiment Design

2.1 Experiment Design

Experiment design is a strategic approach to answering two basic questions about parametric studies: (1) what inputs are specified and (2) what outputs are collected. Although the basic ideas date back to the seminal work of R. A. Fisher, some eighty years ago, experiment design has only recently become established within the aerospace engineering community[5]. Aerospace engineering is not alone as a latecomer to statistical experiment design, as pointed out in the excellent review article of Myers, Khuri and Carter[6]. Several factors have contributed to the relatively limited exploitation of experiment designs, including: a historical association with a few specific industries, communication barriers between academic statistics and applied engineering, and a historical lag between theoretical developments and software capabilities. The last two decades have seen dramatic progress on all three fronts, driven in part by the widespread availability of powerful computing hardware and user-friendly statistical software. Myers, Khuri, and Carter also alluded to the influence of market forces and "...the recent, almost passionate, push for quality and experimental design in industry...." The dozen years since those words were written have given rise to the "better, faster, cheaper era" in aerospace that has resulted in downward pressure on research budgets across the industry[7,8]. The need to maximize "information gained per data point" has lead to an increased interest in DOE for a variety of aerospace applications.

A class of designs, known as response surface methods (RSM), have proven useful for revealing the complex and interacting effects that often appear in engineering systems. System knowledge can be captured in a polynomial regression model. This model can then serve as a surrogate for the complex system response, if properly constructed. These techniques are typically thought of as strategies for a "physical" test program (i.e. wind tunnel tests), as opposed to a "simulated" test program. The last decade, however, has seen the extension of RSM to computer experiments with impressive results.

2.2 RSM and Computer Experiments

The concept of a polynomial RSM based upon "computer experiments" seems to have arisen at least two decades ago[9] for the calculation of pre-mixed flames and reaction rate coefficients. The literature contains several examples of RSM applied successfully to computer experiments. References[10,11,12,13,14,15] demonstrate the variety of aerospace engineering analyses that have benefited from this approach. The present work contains three examples that rely upon CFD solutions of the Navier-Stokes equations for the response data. However, the deterministic nature of these CFD experiments demanded a new approach to error analysis that combined the statistical regression error and acknowledged biases/errors in the CFD results.

Most computer experiments differ from physical experiments in one very significant manner: the computer experiment is a deterministic problem, where as the physical experiment is a stochastic problem with measurement uncertainty. This attribute calls into question the appropriateness of standard regression-error-analysis for computer experiments, in the absence of a normally distributed error[16]. However, traditional lack-of-fit statistics can be used to quantify the agreement between the polynomial model itself, and the underlying response data used to build the model. Our approach has been to quantify the acknowledged modeling errors (i.e. grid dependence, iterative convergence, turbulence modeling dependence, artificial diffusion coefficients, etc.) and combine these with the statistical error (95% confidence interval on future prediction of the response). Experience has shown that the construction of a regression model, with prediction errors comparable to the modeling errors/biases, can be accomplished. This approach has focused the conclusions upon the trends that are clearly significant, when compared to both regression and modeling errors. Confirmation testing of a RSM's predictive capability can quickly assess the validity of the general error statement. Section 5 describes this process in some detail, although this approach to error analysis has been applied to all three studies discussed below.

Statistical science has begun to develop an alternative approach to experimental design for deterministic problems. Design and Analysis of Computer Experiments (DACE) is based upon kriging methods from the spatial statistics literature[16,17,18,19]. DACE strategies strive for "space filling" designs, as opposed to classical strategies based upon symmetric, rotatable, and optimal form designs. The most striking difference with traditional designs involves the lack of design point replication. This gets at the heart of deterministic versus non-deterministic experiment designs: computer simulations should be reproducible to machine accuracy. DACE response models differ from traditional (polynomial-based) response surface models because they possess the ability to interpolate the data. This feature can be advantageous when the deterministic nature of computer experiments is considered. It is often said that DACE methods can "honor the data." However, Papila and Haftka[15] point out that engineering analysis can benefit from the inherent smoothing of polynomial-based response models when other numerical noise sources are present. Sasena[20] includes a good general discussion of DACE methods, contrasting this approach to several other well-known techniques for global optimization. Giunta and Watson[21] make direct comparisons between the polynomial RSM and DACE for several mathematical test functions. Simpson et al[22] have compared polynomial RSM and DACE for the multidisciplinary design optimization of an aerospike nozzle configuration, using both CFD and structural analysis. These comparisons highlight the complimentary nature of these design strategies. In general, the polynomial-based methods will work well when the underlying assumptions of smooth variation are present. Predictive capabilities have been similar between the two, for this class of problems. DACE methods appear to have a distinct advantage for modeling a design space where extreme non-linearity is expected.

The objective of this work was to demonstrate how RSM and CFD have been incorporated into a technology maturation process for the GTX propulsion system. Three different sub-system models have been discussed: the inlet total pressure recovery during hypersonic flight, the fuel mixing efficiency during scramjet mode, and the expansion system during all-rocket mode. Different experimental objectives have led to three different experiment designs. The resulting regression models have been incorporated into the overall system-level analysis, albeit in different ways. The inlet recovery model was used for a performance map of the hypersonic flight regime, where extensive ground testing was too costly. Likewise, the model of fuel mixing was used to screen injector designs for the hypersonic flight regime, where test data was difficult to obtain. Finally, the model of specific impulse efficiency was used to develop a performance map and an understanding of the governing fluid physics. The paper has been organized into three separate sections. A few common themes that relate uniquely to DOE and CFD will be discussed at the conclusion of the paper.

3 Hypersonic Inlet Analysis: Predicting System Performance

3.1 Background

The GTX inlet (station #1 to #2 of Figure 1(b)) was based upon a mixed-compression design. A small amount of initial compression from the vehicle forebody was accounted for as well[23]. Initial inlet performance of a 12 degree conical design has been tested and widely reported[24,25,26,27]. After design modification of the inlet flowpath, a new performance map was required for the inlet. Thus a second series of CFD analysis and supersonic wind tunnel testing was initiated. The difficulty of hypersonic testing has lead to our reliance upon CFD during this portion of the ascent trajectory.

3.2 Experiment Design

The emphasis upon highly precise performance prediction has lead to a relatively dense full-factorial experiment design in two parameters: flight Mach number (M) and inlet contraction ratio (CR). A graphical representation of the experimental matrix is shown in Figure 2. The primary response variable of this study was a regression model of inlet total pressure recovery. The experimental design space covered the expected range of practical inlet operations during scramjet mode. The freestream Mach number ranged from a six to twelve, while the inlet contraction ratio ranged from eight to sixteen. We have assumed that an adequate regression model could be assembled from linear, quadratic and bi-linear (simple interaction) terms; all higher order terms and interactions are assumed to be zero.

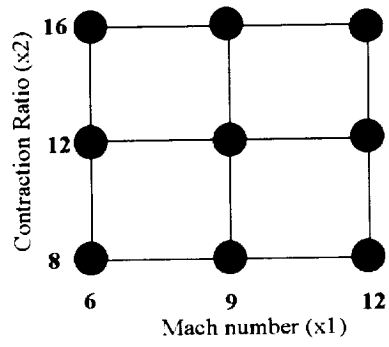

Figure 2 Experimental design schematic

3.3 Numerical Modeling

The flow solver GASP v3.2[28] from AeroSoft, Inc. was used to conduct the non-equilibrium, finite rate analysis. The numerical modeling was similar

to an earlier study[24]. From the earlier work, the grid resolution requirements for this work were well understood*. The present calculations were run on one of three (325 axial by 99 radial) meshes, according to the required contraction ratio. The numerical models were the same as documented in the earlier work, with the exception of two boundary conditions. The freestream boundary that lies parallel to the incoming flow was either modeled as a slip wall or as a shared block interface, depending upon whether the inlet flow spilled. Thus, for a spilled flow situation, resolution of the external flow over the cowl was required. The single configuration that spilled was the minimum speed, minimum contraction ratio case (i.e., Mach=6, CR=8). The other boundary condition modification was the inclusion of a section of isothermal wall in the portion of the internal flow regions. The entire cowl (leading edge to throat) and a portion of the centerbody (cowl shockwave to throat) were cooled. The specified wall temperature was 900R at M=6, 1200R at M=9, and 1500R at M=12. The output of the CFD calculations was stream thrust averaged, and the stagnation conditions were evaluated with the Chemical Equilibrium Analysis code[29]. As noted above, the primary response variable was inlet recovery. A secondary response variable, heat transfer per-unit of capture area, was also modeled for this configuration. The data matrix is included below in Table 1.

	Case1	Case2	Case3	Case4	Case5	Case6	Case7	Case8	Case9
Mach #	6	6	6	9	9	9	12	12	12
C.R.	8	12	16	8	12	16	8	12	16
Recovery	69.20%	69.59%	68.73%	29.95%	26.23%	24.99%	12.83%	9.99%	9.72%
Heat Trans. (btu/ft²/s)	188.76	230.44	190.74	439.65	559.7	552.03	816.64	1033.0	1113.9

Table 1 Inlet design response data

3.4 Results

The flow visualizations are summarized below (see Figure 3) in a series of images depicting the shock structures. The shock-on-lip condition occurred at the (Mach=6,Contraction Ratio=12) case. The (M=6,CR=8) spills slightly, while the remainder of the cases are over-sped to some degree. Detailed discussions about the operation of this inlet are given elsewhere; the following discussion will concentrate on the statistical regression results.

Regression analysis was conducted with Design Expert[30], and the two models are given separately, below. First the recovery model is given by the following formula: $\frac{P_{02}}{P_{01}}(\%) = 235.37 - 35.624 * M - 0.3558 * CR + 1.439 * M^2$ with $E \approx \pm 3\%$ @ 95% confidence.† This prediction error estimate is based upon the standard error of regression $S_{Y.X} = \sqrt{\frac{\Sigma\left(Y - \hat{Y}\right)^2}{(dfE)}}$, and the Student's t-distribution[31]. The response surface can be visualized in a 3D carpet plot. The graphic results of this response clearly indicate the important role played by Mach number. The relatively small influence of contraction ratio can be seen in the data as well.

* The grid convergence index was (0.928%) for a grid-doubling analysis of the total pressure recovery. For more on the GCI, see section 5.3.

† This model was the simplest of several *very* similar regression models that can be fit through the same data. This approach has an assumed even distribution of errors, which may raise some concern. An analysis that square-root-transformed the recovery data, generates an error estimate that scales with the recovery data itself.

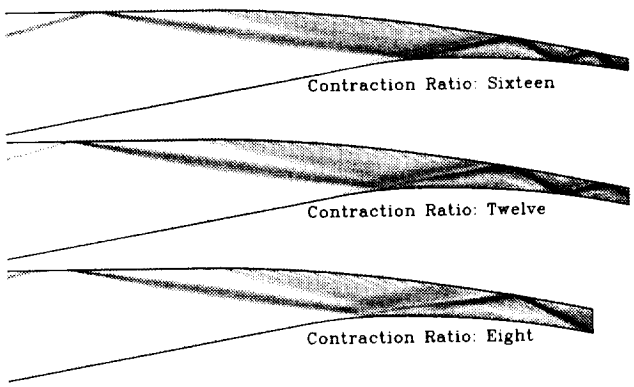

(a) Mach 6 Results

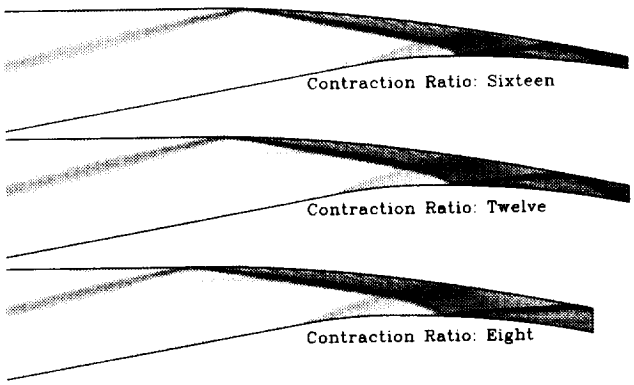

(b) Mach 9 Results

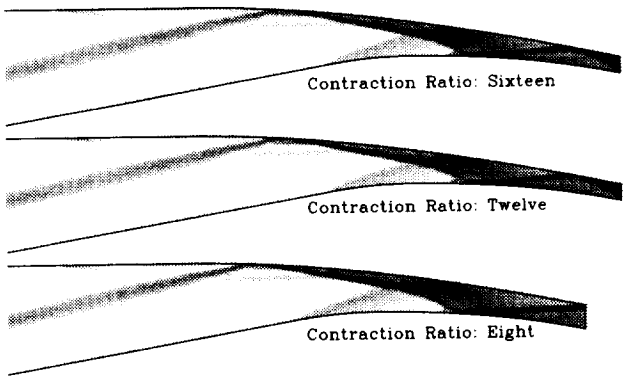

(c) Mach 12 Results

Figure 3 Hypersonic Inlet flow: numerical schlieren

The heat transfer data was best resolved with a square-root transformation. The model form is given by the following formula:

$$\sqrt{Q_{1-2}} = -7.07414 + 1.67187 * M + 1.42005 * CR - 0.083250 * CR^2 + 0.098466 * M * CR$$

with $E \approx \pm 0.31$ @ 95% confidence. This error statement is based upon the standard error of regression, in transformed units: $S_{\sqrt{Y}.X} = \sqrt{\frac{\Sigma\left(\sqrt{Y} - \sqrt{\hat{Y}}\right)^2}{(dfE)}}$. A dominant effect of Mach number was quite visible in both the raw data and response model. The interaction of contraction ratio and Mach number was, perhaps, an unintended complication of the experimental setup. The actual amount of cooled wall area differed at each CR value. This amounts to a "bookkeeping" issue of where the inlet throat occurs, and clouds the proper interpretation of contraction ratio effect. One would expect that at a given flight condition, a higher contraction ratio would yield a higher pressure and temperature environment and thus more heat transfer. However, because the amount of cooled wall modeled in this study varies in a non-linear fashion, this effect was not clearly illuminated with this DOE. This issue highlighted the point that a DOE, configured with one response in mind, may not adequately address a secondary response variable. Below Figure 4 shows the response surface results for both recovery and heat transfer.

In summary, results indicated that the effect of Mach number upon the two response functions (recovery and heat transfer) was significant. The effect of contraction ratio was small but statistically significant for both the recovery and the heat transfer models. Since the statistical error was significantly larger than the errors associated with either mesh dependence or iterative convergence (both under 1%), a general prediction error was set equal to the statistical prediction errors, for both models. The two models can be used as accurate surrogates for further CFD simulation within the experimental design space.

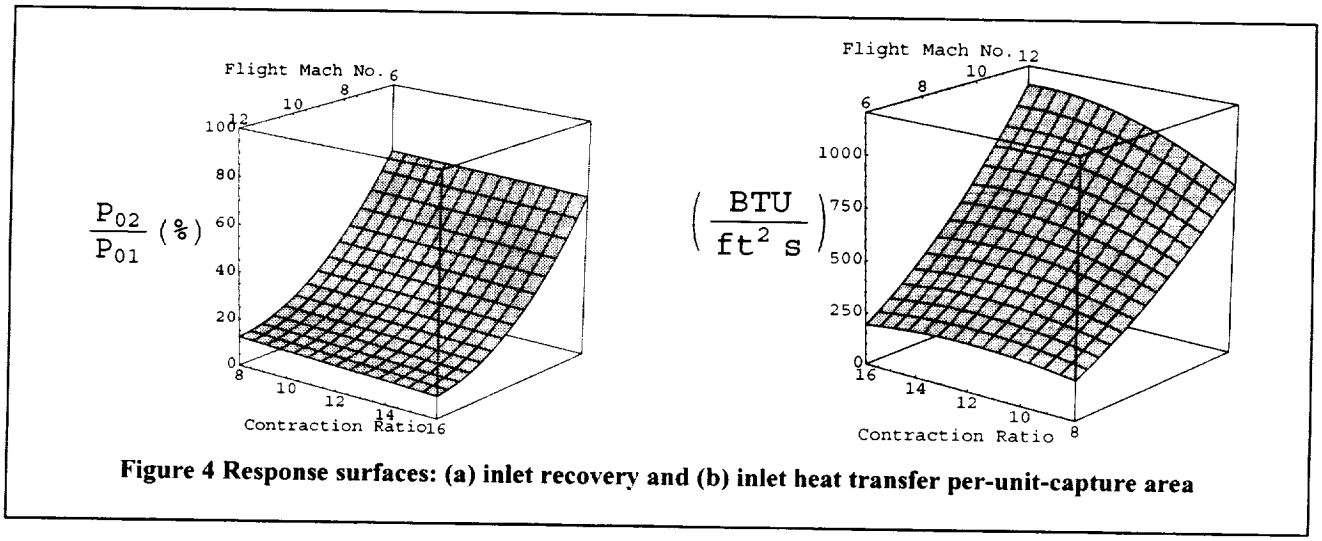

Figure 4 Response surfaces: (a) inlet recovery and (b) inlet heat transfer per-unit-capture area

4 Scramjet Combustor Analysis: Screening Important Effects

4.1 Background

The GTX flowpath presents a design challenge for the air-breathing combustor (see Figure 6(a)). Fuel injection ports will be used for both the low speed IRS cycle and the scramjet cycle. Parametric analysis is underway to help define the performance implications of different injector design patterns. CFD offers an efficient method, when coupled with ongoing experimental efforts, to estimate combustor performance. It is widely recognized that the significant advantage of CFD analysis, for scramjet flows, lies in the ability to quickly examine a broad variety of geometric parameters at full scale and flight enthalpy. Extensive ground testing of these systems is prohibitively expensive. Of course, CFD has several inherent limitations when modeling these flowfields, and results must not be misinterpreted as the definitive answer. CFD has been widely used for scramjet design studies[32] to gain insight into this complex trade space.

The goal of this study was to assess which fuel injector design parameters have the most impact upon the hydrogen fuel mixing. Initial CFD analysis of the GTX scramjet combustor has been executed for a variety of conditions[33]. However, after reviewing these separate cases, no clear optimum configuration was apparent. Several fuel-injector design parameters appeared to have significant, interacting effects upon performance. A second set of CFD calculations, organized around a DOE matrix, has been conducted. Unlike the earlier analysis, the present calculations were executed as mixing studies on relatively coarse three-dimensional meshes. Mixing analysis implies that no reaction between the hydrogen (H2) and oxygen (O2) was modeled. This approach was based upon the assumption that the scram combustion process was mixing-limited. This approach has been employed to study high-speed fuel injection schemes before with good success[34,35]. Another difference from earlier analysis was the reliance upon coarse mesh results for building a response surface model. Two levels of mesh refinement have been examined for these problems: a coarse level (280k cells), which is every-other-point of a related fine level mesh (2.240M cells). Previous mesh dependence analysis indicated that the coarse results underpredict the fine mesh results for combustion efficiency by approximately five-percent. Reliance upon coarse mesh results enabled an extensive design space for experimentation, yet restricted the interpretation of the RSM results. Conclusions have been limited to (1) screening significant design parameters, and (2) highlighting regions of design space for further refinement. These compromises enabled a relatively large study (5 parameters at 3 levels) to be conducted in the time allotted, while still modeling the three-dimensional mixing process.

The concept behind the current scramjet combustor design includes two different fuel injection locations. The first set of injectors were placed at station #2 and constituted the "streamwise" injection ports, located in the backstep region of both the cowl and centerbody. They were spaced around this annular region at a 1.5-degree pitch. These streamwise injectors fueled the flame holding region of the combustor and perhaps, supplied a substantial portion of the required fuel. The second set of fuel injectors, wall mounted "transverse" injection ports, were placed in the constant area portion of the scram combustor flowpath (see Figure 6(a)). The transverse injectors were located along both the cowl and centerbody at a given station, spaced at a three-degree pitch.

Note that the CFD domain extended from station #2 to station #3, and simulated a 1.5 degree slice of a full 360-degree annular geometry. By contrast, the combustor hardware was approximately 220 degrees, with planar endwalls. We have assumed that endwall effects were of secondary importance to this study, and therefore have been neglected.

4.2 Experiment Design

The GTX propulsion system has a combustion efficiency target of 92.5% throughout the scramjet mode operation. This target efficiency must be achieved at a combustion exit plane that varies throughout the scramjet portion of trajectory. This goal was approximated with a mixing efficiency target of 95% at station #3. The definition of mixing efficiency for this study is given by the percentage of *oxygen* that would be present in product water, if the flow was allowed to reach chemical equilibrium without further mixing. The species oxygen has been used because all of the conditions within the study are stoichiometric or fuel rich.

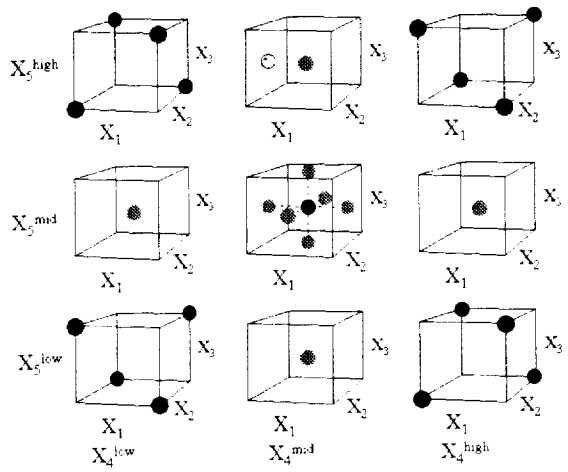

Figure 5 Scramjet mixing study: design schematic

Case #	Step Injector %	Wall Injection Angle (deg)	Wall Injection placement	Mach #	Fuel/Air ratio ϕ_{total}	η_{mix} (%)
1	25%	15	fwd	6.5	1.4	94.1
2	75%	75	fwd	6.5	1.4	63.9
3	25%	75	fwd	6.5	1	76.0
4	75%	15	fwd	6.5	1	41.2
5	50%	45	mid	6.5	1.2	75.7
6	75%	15	aft	6.5	1.4	41.3
7	75%	75	aft	6.5	1	44.3
8	25%	15	aft	6.5	1	61.3
9	25%	75	aft	6.5	1.4	91.7
10	50%	45	mid	9.25	1	61.3
11	50%	45	mid	9.25	1.4	74.1
12	25%	45	mid	9.25	1.2	84.5
13	75%	45	mid	9.25	1.2	43.2
14	50%	45	mid	9.25	1.2	67.5
15	50%	75	mid	9.25	1.2	71.0
16	50%	45	aft	9.25	1.2	47.3
17	50%	45	fwd	9.25	1.2	51.6
18	50%	15	mid	9.25	1.2	54.5
19	25%	15	fwd	12	1	75.2
20	75%	75	fwd	12	1	51.5
21	25%	75	fwd	12	1.4	86.8
22	75%	15	fwd	12	1.4	55.3
23	50%	45	mid	12	1.2	62.8
24	75%	15	aft	12	1	34.7
25	75%	75	aft	12	1.4	44.1
26	25%	15	aft	12	1.4	52.6
27	25%	75	aft	12	1	47.5
28	25%	45	mid	9.25	1.4	88.8

Table 2 Experimental matrix for fractionated CCD

The emphasis here upon rapid analysis of many potential fuel injector design parameters has lead to a relatively sparse, fractionated central composite design (CCD) in five variables (see Figure 5). This specific design was implemented in two distinct phases, as represented by the two different colored dots in Figure 5. The black dots represented a fractional-factorial-plus-centerpoint (screening) design, while the additional gray dots enabled a more complete response surface model. The single clear dot represented the confirmation case (number 28), which is discussed in section 4.4. The five design variables were:

X1: Fuel split between step injectors and wall injectors (25%-75%, 50%-50%, 75%-25%); see Figure 7

X2: Wall fuel injection angle (75deg, 45deg, 15deg); see Figure 6(c)

X3: Wall fuel injection placement (fwd, mid, aft); see Figure 6(b)

X4: Flight Mach number (6.5, 9.25, 12)

X5: Total fuel/air ratio (1.0, 1.2, 1.4)

The 17 case screening design was completed and the resulting model revealed 5 significant main effects and 2 interactions. A decision was made to continue with the full 27-case study to explore the quadratic effects of these five design parameters. The following discussion related specifically to the analysis of the full 27-case response model. Note that several different response variables can be modeled from the 3D RANS data of this study, including a variety of mixing efficiencies and loss measures. I have confined my remarks to a discussion of the mixing efficiency at station #3. The statistical analysis was carried out with Design Expert.

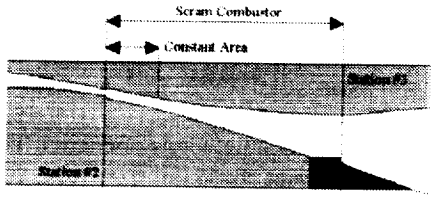

(a) Scramjet combustor flowpath

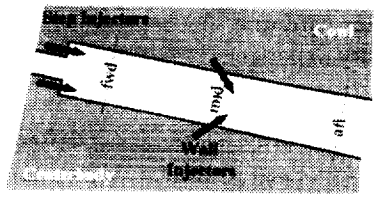

(b) Three wall-injector locations

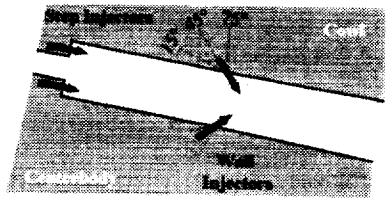

(c) Three wall injector angles

Figure 6 Scramjet combustor geometry

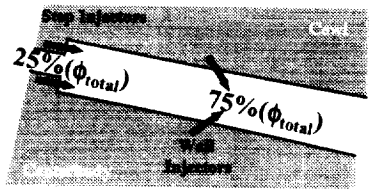

(a)

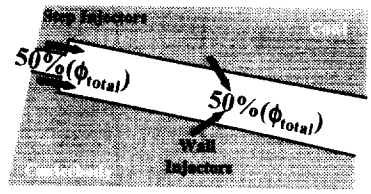

(b)

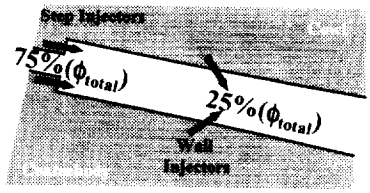

(c)

Figure 7 Hydrogen fuel distribution scheme: (a) 25% step fuel, (b) 50% step fuel, (c) 75% step fuel

4.3 Numerical Modeling

The numerical modeling employed for this study was considerably different than prior scramjet analysis[33]. The primary change was the use of a new version of the GASP solver (version 4.0)[36]. GASP is a 3D, finite volume, structured-mesh RANS solver that has been used to analyze many high-speed propulsion flows, including scramjet combustors, in steady state or time-dependent fashion. The solver was specified as follows:

- Time integration: steady state analysis with Gauss-Seidel implicit method and inner iteration scheme (Gauss-Seidel, again)
- Inviscid flux function: Van Leer scheme with MUSCL reconstruction (κ=1/3) and the minmod limiter function
- Laminar transport properties: Sutherland's law was used for modeling viscosity and thermal conductivity, while mass diffusion was modeled as a constant-Schmidt-number flow
- Turbulent flow model: full 3D viscous analysis, Wilcox '98 k-ω model[37], with turbulence modeling limited as follows: $\mu_{turb} \leq 2000\mu_{laminar}$; turbulent Prandtl and Schmidt numbers are both set to value of 0.5
- Chemistry model: frozen 3-species (N2, O2, H2) and NASA GRC thermal equilibrium database
- Boundary conditions: injectors modeled as sonic (fixed condition) H2 jets; combustor walls modeled as adiabatic no-slip walls; combustor inflow modeled as supersonic inflow (fixed condition) that was calculated a priori; symmetry condition applied at both spanwise boundaries; extrapolation outflow boundary.

The mesh was slightly finer than the earlier study, and the results were run on a coarse sequence of (140 axial, 100 radial, 20 spanwise) cells, as discussed above. A fine mesh, used to quantify the mesh dependence, was doubled in each direction (280x200x40). The mesh dependence observed at the design centerpoint (case 14) was 4%. This result agreed with earlier analysis[33] of mesh dependence for these flowfields. The geometry was modeled at the reference vehicle scale, as opposed to the (8.5%) model scale used in the earlier study. All results have been converged so that massflux was constant to within ($\pm$1%). This convergence takes approximately 4500 iterations on the coarse mesh, and another 2500 iterations on the fine mesh. The coarse mesh result took approximately 900 cpu hours (SGI R12k 400mhz) on a 16-cpu O2000 machine. This translated into approximately 2.3 days of wall-clock time.

4.4 Results

Figure 8 shows three examples of the three-dimensional mixing results within the dataset. The images depict the flowpath (between stations two and three) with cross-section slices of local fuel/air ratio. The small dark ports on the centerbody geometry clearly indicate the location of the wall injection holes. The cowl (not shown) had similarly located injection ports. The regions with fuel-rich conditions appeared as black; likewise the white regions depicted the complete

absence of any fuel. For effective fuel mixing, one would expect to see a uniformly dark cross section at the combustor exit plane. Poorly mixed results tended to concentrate the hydrogen fuel in the near-wall region, which resulted in a band of white (unmixed oxygen) along the centerline of the flowpath. The natural interpretation of this stratified result was poor fuel-jet penetration into the high-speed core.

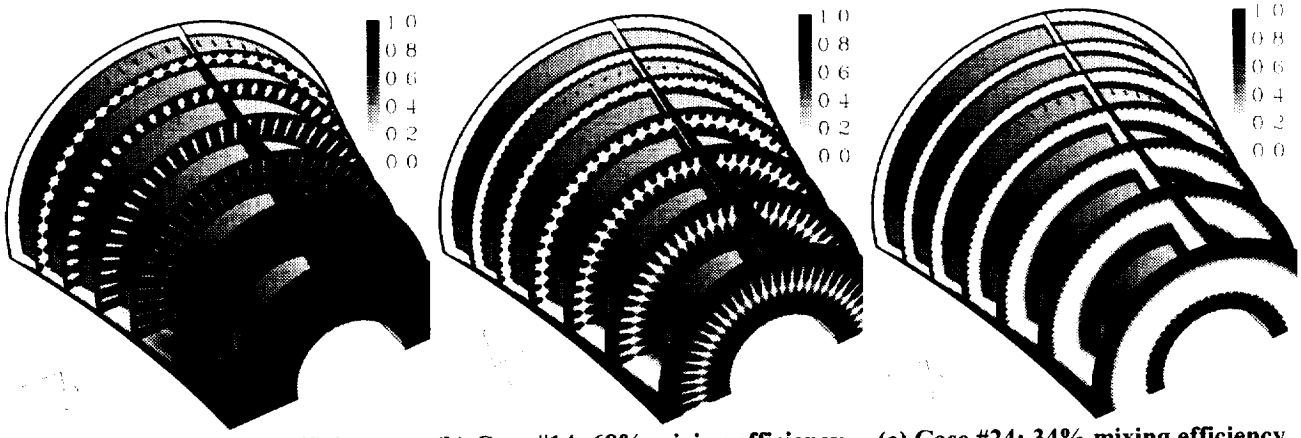

(a) Case #1: 94% mixing efficiency **(b) Case #14: 68% mixing efficiency** **(c) Case #24: 34% mixing efficiency**

Figure 8 Three-dimensional flowfield contours of local fuel-air ratio

The observed station #3 mixing efficiencies varied from 34%-94%. This broad range of "percentage" results required a transformation of the data, prior to modeling. The transformation was of the form: $\ln\left[\frac{\eta_{mix}}{100\%-\eta_{mix}}\right]$. This confined the mixing efficiency model to the meaningful range of [0,100%].

The regression model that resulted from this work contained five significant linear effects, two quadratic effects and four bilinear interactions. Several significant trends are described below in a series of three carpet plots. Overall, the regression model pointed to a distinct region in design space that deserves further refinement and optimization.

Figure 9 revealed two of the strongest trends in the data: the influence of Mach number and total fuel/air ratio upon mixing performance. In general, mixing performance improved with increasing levels of (ϕ). This trend is well known for scramjet combustors. Likewise, the performance was observed to be inversely proportional to freestream Mach number. Figure 9, which cut through a region of high mixing efficiency within the design hyperspace, suggested that the target of 95% was only realized at the minimum Mach number and maximum fuel/air ratio.

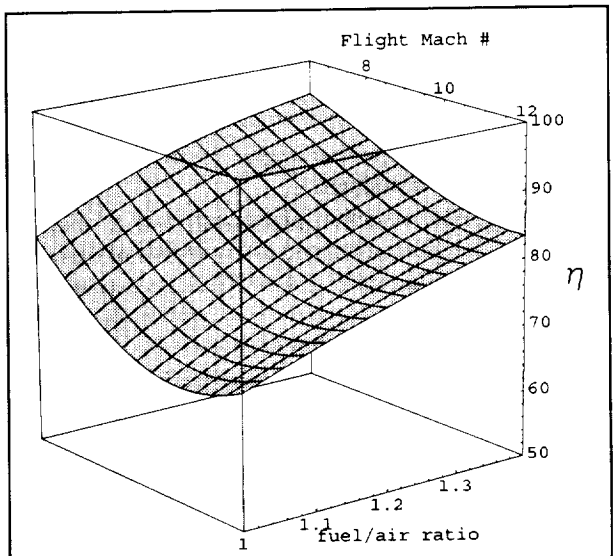

Figure 9 Scramjet mixing response surface: mixing efficiency as a function of Mach number and fuel/air ratio

Figure 10 reveals another strong trend in the data: the influence of the fuel distribution between streamwise and transverse injectors. For all Mach numbers, performance was maximized when the majority of the H2 was injected thru the transverse injectors. This result was intuitive, because a jet-in-crossflow has better near-field mixing than a comparable co-flowing jet.

Figure 11 revealed another important aspect of the data: the minor influence of transverse injection angle and location. Figure 11 depicted the mixing efficiency as a function of the transverse injection angle and location for three different Mach number conditions: the white surface represented Mach 6.5 flow, the gray surface represented Mach 9.25 flow and the dark surface represented Mach 12 flow. Notice that the response surfaces were relatively flat for the region defined by the fwd-mid injector location, at all injection angles (15-75deg). This

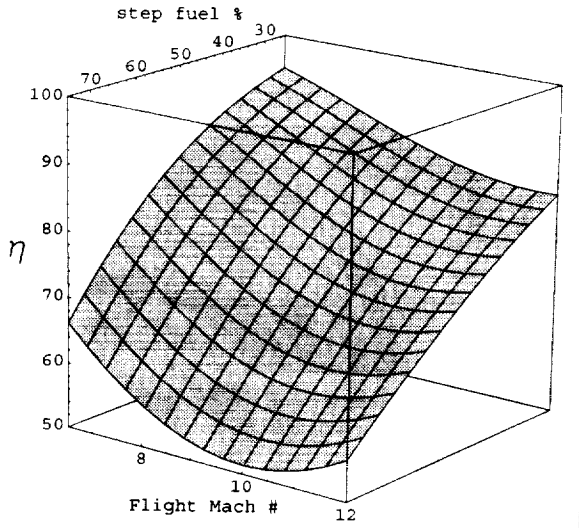

Figure 10 Scramjet mixing response surface: mixing efficiency as a function of Mach number and step fuel percentage

implied that injector definition within these bounds could be driven by other performance constraints, such as minimization of total pressure loss. One might expect the dramatic penalty observed for injecting the fuel at a minimum angle (low penetration) from the furthest point downstream (aft end of constant area combustor). This configuration had little chance of fueling the high-speed core flow. Increasing Mach number appeared to exacerbate this penalty. The primary conclusion, drawn from the trends evident in Figure 11, was this: a single transverse injector design (location and angle) can be used to achieve relatively good mixing performance across the Mach number range.

Thus far, confirmation of the predictive capability of this response model has been examined at one location within design space (see case 28 of table 2). The observed CFD result (88.8% mixing efficiency) was in good agreement with the RSM prediction of (86.9%), and well within the ninety-five-percent confidence interval of [79.1%,92.1%]. This result merely suggests that the response model can serve as a surrogate for the coarse mesh results. In general, the 95% confidence interval for prediction was neither constant nor symmetric within design space. This was a result of the natural-logarithm transformation. Since the response model was built upon data with a significant mesh dependency, it should *not* be used as a surrogate for future CFD results within this entire design space. Rather, a second RSM analysis should be conducted in the region of high mixing efficiency with fine mesh resolution. This second model should yield a highly reliable surrogate appropriate for design optimization.

In summary, a polynomial model of mixing efficiency has been constructed from 27 coarse mesh solutions of a 3D scramjet combustor. The study included five parameters important to fuel injector design. All five parameters appeared as significant factors in the response model of mixing efficiency. The mixing efficiencies were observed to span the range from 34% to 94%. The fidelity of the coarse mesh simulations was adequate for screening the design variables and identifying regions of high mixing efficiency. A distinct region in design space appeared to hold the most promise for maximizing the mixing efficiency, across the Mach number range. This region was defined as follows:

- Fuel split between step and wall injectors: 25% step and 75% wall, or X1 set to minimum value.
- Wall injection angle: 15 to 75 degrees, or X2 unconstrained.
- Wall injection placement: fwd to mid location, or X3 constrained to lower-half of design space.
- Fuel-air ratio: 1.4, or X5 set to maximum value.

An analysis of total pressure loss within the flowfield is expected to narrow the region of interest for injector location and angle (X2 and X3). Follow-on analysis can now focus upon a reduced design space (Mach number and fuel-air ratio) to develop a performance map of mixing efficiency in the region of interest. One would expect the results from the next phase to be more tightly clustered around 95% efficiency. This should greatly reduce the ninety-five-percent confidence interval of prediction, while demanding a higher level of numerical fidelity in the CFD analysis. The fine-mesh analysis is required for this next design iteration, which can be accomplished in five CFD experiments.

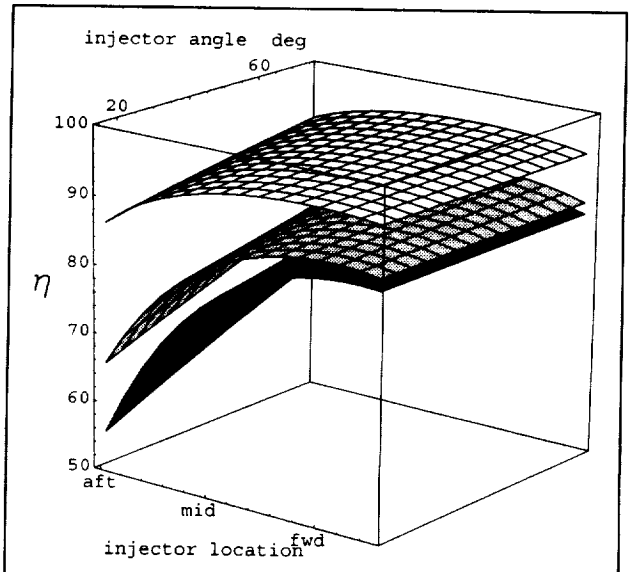

Figure 11 Scramjet mixing response surface: mixing efficiency as a function of transverse injector angle and location at Mach 6.5 (white), Mach 9.25 (gray) and Mach 12 (dark)

5 Rocket-Mode Performance: Prediction and Uncertainty Analysis

5.1 Background

Vehicle performance is highly dependent upon the efficiency achieved during the fourth and final propulsion mode. This is due to the fact that the largest portion of the ascent trajectory is flown with the inlet closed and the rocket turned on. However, the literature on this all-rocket mode is relatively sparse. Most studies of RBCC systems have focused their experimental efforts upon the air-breathing sub-system performances, and assumed some value of expansion efficiency for the all-rocket mode. This was primarily due the costs associated with simulating this high-speed, high altitude flow with a ground test. We have chosen to initially investigate this fourth mode with CFD. We attempted to reveal the most critical design parameters for further investigation and optimization. A generic RBCC engine geometry was specified with similar attributes to the GTX system (see Figure 12). The emphasis here upon screening a large number of potential design parameters lead to a 36-case D-optimal experiment design in six variables. The specific objectives were to:

1. Determine the most critical design parameters that influence performance for further analysis.
2. Develop an initial predictive capability for impulse efficiency for incorporation in the GTX design cycle.
3. Apply flow visualization to examine the predominant fluid dynamic effects.

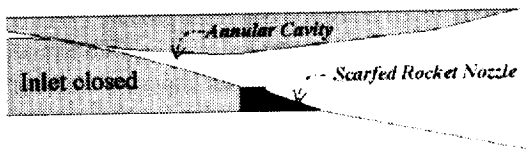

(a) Flowpath geometry for mode 4 (all-rocket)

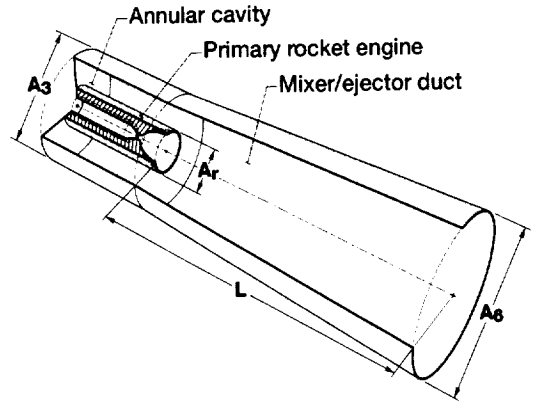

(b) Axisymmetric RBCC nozzle geometry

Figure 12 RBCC nozzle geometry: (a) GTX flowpath and (b) simplified axisymmetric geometry with four geometric parameters

The axisymmetric, Reynolds-averaged Navier-Stokes simulations were executed with the NPARC v3.0 code. A response surface was created for specific impulse (I_{sp}) efficiency, based upon data integrated from the 36 CFD simulations. Thirteen statistically significant effects were observed to have an influence on RBCC nozzle performance. The results of this effort have been widely reported[13]. The following discussion outlines the uncertainty analysis undertaken. This analysis incorporated several sources of modeling bias together with the standard error of regression, to develop an overall uncertainty bound on the *precision* of this effort. Our goal was to report an uncertainty bound for the response model that was representative of these acknowledged errors.

At the outset of this study, the authors sought to avoid modeling effects that appeared in the results at a level associated with grid dependence, choice of turbulence model, selection of convergence criterion, and specification of numerical viscosity coefficients. These were assumed to be the critical components associated with "noise" in the results. Our goal was to quantify the influence of these items, and seek to fit a regression model through the data with a predictive error that approximated this "noise" level. This was an informal approach to insuring that our results were robust to the arbitrary specification of these numerical modeling parameters. The advantage of this approach was that it permitted the familiar error statement and confidence interval to be defined according to classical theory. The disadvantage was the implied assumption of a stochastic response, which is not strictly valid. An unavoidable consequence of publishing an approximate predictive error of regression was the need to run some confirmation cases within the design space and examine the residuals.

5.2 Turbulence Modeling Bias

We quantified the difference in performance prediction, between a robust one-equation model and a widely applied two-equation model, with an analysis of variance (ANOVA). A six-parameter screening design (nine-run Plackett/Burman-plus-centerpoint) was repeated with each turbulence model to allow a direct assessment. Analysis of Variance (ANOVA) techniques were applied and we concluded that the two multiple-linear-regression (MLR) models agreed very well. The

single significant difference was in the definition of the intercept value: the two-equation model consistently predicted results that were 1% higher than the one-equation model.

5.3 Grid Dependence Bias

Grid dependence is an un-avoidable consequence of modeling continuous physics with discrete mathematics. Furthermore, there is a variety of ways to report this artifact of CFD calculations. One approach to uniform reporting mesh sensitivity of CFD results has been gaining acceptance by the engineering community[38]. This reporting technique is referred to as the Grid Convergence Index. The GCI is not a bound on the error; rather it is "...a reasonable error band, in the flavor of a statistician's 2σ range or an experimentalist's 20:1 odds...." The GCI accounts for the order-of –accuracy of the CFD solver. An evaluation of grid dependence for our primary response variable was assessed at the centerpoint of design space. The assessment compared a standard resolution of 56,952 points with a fine resolution of 226,281 points. The raw difference in the response was 0.346% and the GCI value was 1.6%. We have assumed that this value was representative of the entire design space, although twenty-seven different grids were used in the study. In order to support this assumption, we strictly defined the grid generation process, including the multiblock topology, the minimum near-wall spacing, the maximum far-field spacing, and the maximum stretching ratio between adjacent cells. This strict definition of grid development enabled similar discretization of flows through different geometries.

5.4 Iterative Convergence Bias

Incomplete iterative convergence is a practical reality for engineering applications of CFD. At the outset, we addressed the issue of the reported values of I_{sp} and their sensitivity to incomplete iterative convergence. Often overlooked, this issue proved to be non-trivial when considering DOE and CFD. Ultimately, we decided to monitor the primary integral quantities every 100 iterations. The residuals of massflow and thrust converged at least 4 orders of magnitude. Furthermore, we demanded that the value of I_{sp} should not change more than 0.15% over the last 10,000 iterations at a Courant number of 0.5. This criterion required several of the longest domains to be run in excess of 50,000 iterations, depending upon the initial conditions prescribed. The extremely long iteration counts were necessary to resolve the widely varying wave speeds present in a domain with large regions of low speed flow present alongside hypersonic jet flow. In general one should be able to account for the small, but finite time-dependence of a steady-state response variable. Often it is controlled with further iteration upon the numerical solution, so that it is negligible when compared to the other sources of modeling bias.

5.5 Artificial Diffusion Bias

The convective terms of the Euler equations were handled with a central difference scheme. The common approach of Jamison, Schmidt, and Turkel was applied to introduce second- and fourth-order artificial diffusion to control numerical instabilities. The magnitude of artificial diffusion included in a calculation can affect the results. Experience and intuition often guide the specification of these particular coefficients because, as Hirsch[39] correctly points out, "...little information is known on the stability of general non-linear discretized schemes...." Nevertheless, the influence of artificial diffusion upon the response variable is real and can be quantified. For our study, the baseline value of the 4th-order coefficient was (1/100). This was sufficient to stabilize most of the 36 test cases used to build the RSM. An increased value of the 4th-order coefficient (1/32) was required to stabilize a few cases and achieve a steady-state convergence. The influence of this alternate coefficient value upon the response was (0.3%). This value was considerably less than the bias introduced through mesh dependence.

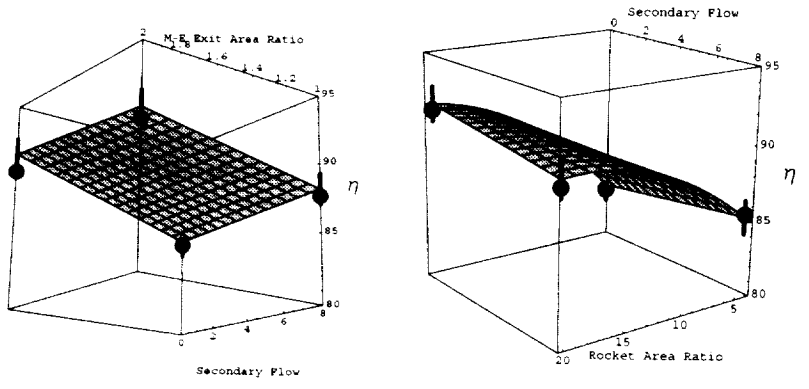

Figure 13 Response surface model confirmation: eight CFD runs, the response surface model, and the uncertainty estimate of (+/-1.1%)

To summarize, the general error statement about predictive capability of this RSM incorporated bias errors introduced from several modeling decisions, as well as the standard error of regression. For this study, it was clear that these considerations consistently pointed to a predictive uncertainty in the range of 1.1%. This combination of modeling and statistical error analysis should focus the

target audience upon statistically significant (and reproducible) trends from the data. The results from eight additional confirmation cases, shown here in Figure 13, bolstered our conclusions in this regard.

6 Lessons Learned

6.1 Communication of DOE Results

Several common themes have emerged from the studies discussed above. One issue of primary importance involved effective communication of the complex statistical results. A concise discussion of significant interactions and second-order effects within a design hyperspace can challenge the most gifted of technical writers (and audiences alike). However, simply creating a regression calculator with a spreadsheet program can allow an interested user to begin exploring the DOE results. If a few interesting extremes are included as regression examples, then often the important trends can be communicated in short order. A more involved approach includes the creation of a short program for use with one of the many graphical mathematical software packages[40]. A third option involves the construction of a custom graphic-user-interface (GUI) that can *graphically* portray some important aspects of the regression model in real time. Figure 14 shows a basic JAVA program used to investigate the RSM results of section 5. This GUI-based approach has several distinct advantages:

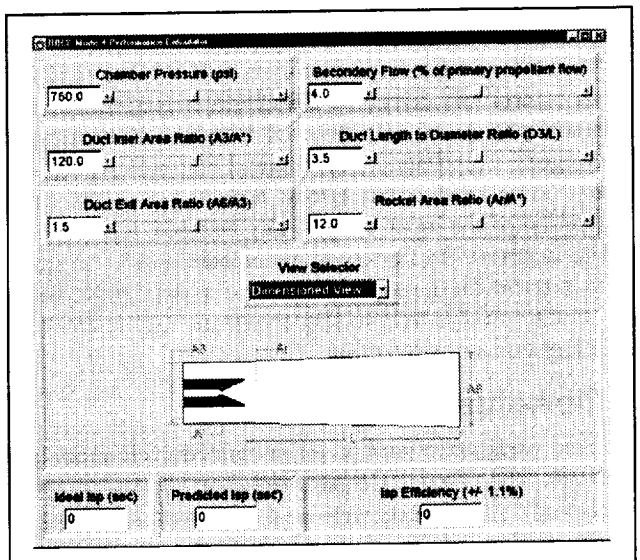

Figure 14 Example of a JAVA program to aid in communication of DOE results

- A single version of the regression model can be made available to a wide audience, via the world-wide-web.
- Explicit parameter limits can be imposed upon the independent variables, preventing extrapolation.
- Familiar browser tools (buttons, sliders, etc) can be used to quickly assemble a custom tool.

Any one of these approaches can be used to make RSM results more approachable to an interested audience.

6.2 Response Models of Integrated CFD Data

Application of RSM techniques has thus far been confined to response variables based upon integrated, multi-dimensional CFD data. This type of data has an inherently smoother nature than either local or peak-value flow data. Integral data is less susceptible to the local nonlinear behavior that is common in multidimensional CFD results. The source of this non-linearity can vary from the mesh-generation for complex geometries, to the numerical resolution of shock waves and contact discontinuities.

6.3 Polynomial-based Response Models and Uncertainty/Bias

Thus far, the acknowledged modeling bias errors have been approximately the same magnitude as the statistical regression uncertainty. In some sense, this has occurred by design because knowledge of the modeling bias was exploited during the model building process. In general, the numerical modeling precision should be matched to the expected statistical regression errors. Consider the effect of running very costly CFD analysis and encountering a modeling uncertainty (i.e. grid dependence) that was far less that the statistical prediction error. This would imply that the mesh dependence could have been increased appropriately without affecting the engineering value of the response model. Likewise, a RSM prediction error that is substantially smaller than the grid dependence would indicate that further mesh refinement is required before the RSM acts as a reasonable surrogate for the CFD solutions. This is precisely what occurred in the mixing analysis of section 4.

Progress with the quantification of modeling errors and uncertainty has received a great deal of attention. The AIAA Committee on Standards for CFD has recently published a guide intended to help assess the credibility of modeling and simulation in CFD[41]. Shih, Gu, and Chu[42] have helped to develop grid quality measures and error estimates for both structured and unstructured meshes. Oberkampf et al[43] and colleagues at the Sandia National Labs have begun to present a very comprehensive framework for discussing "total uncertainty" in the realm of modeling and simulation. These are but three examples of research aimed at quantifying uncertainty and bias for computer experiments.

6.4 Computer Experiments and Process Control

A final comment concerning quality control was relevant to the implementation of these designed experiments. A modern CFD solver has a very large set of independent parameters that require explicit specification prior to simulation. For instance, a typical namelist-input file for one of the GASP v4 mixing calculations of section 4 included 642 different variables; the grid generation process was another separate source of variability. W. Edwards Deming stated that quality process control was driven by effectively managing system inputs, and *not* by mass inspection of system outputs[44]. While this lesson was specifically directed at industrial manufacturing processes, it is just as relevant to the successful execution of a designed experiment. I have found that automating the setup and execution of these repetitive studies was invaluable for controlling inadvertent errors. Simple pre-processing of the experiment can save time and cost by averting mis-specification of the input vectors. For instance, a list of schematic drawings that highlight the critical geometric variations can help to ensure the fidelity of an intended mesh. An automatically generated check-sheet for setup of flow conditions can help to prevent the mis-specification of a simulation, before the computer time is spent. Real-time output of incomplete CFD results can also help to flag erroneous runs at an early stage. Efforts spent upon error prevention have been less time consuming than error detection.

7 Conclusions

Three parametric studies on combined-cycle-propulsion components have been executed in a designed-experiment framework. The computer experiments were executed with different Reynolds averaged Navier-Stokes solvers. The multi-dimensional CFD datasets were post-processed for integral performance measures, which in turn, were used to assemble a response surface model. A response model of CCP component performance can serve as surrogate for further CFD experiments, when a design optimization is undertaken. The three response surface models described in the present work have contributed to the technology maturation phase of the GTX CCP program at NASA Glenn Research Center. The hypersonic inlet recovery model has been used to predict the compression system performance throughout the hypersonic portion of the trajectory. The Scramjet mixing model has been used to screen fuel injector designs that maximize fuel-air mixing and identify promising regions of design space for further analysis and testing. The model of specific impulse efficiency, for RBCC all-rocket mode, has been used to predict system performance and identify performance trends that deserve further attention. All three have led to increased fidelity in the GTX propulsion system design and analysis. The combination of response surface methods and computational fluid dynamics can provide an important design and analysis capability to the development of modern propulsion systems.

References

[1] Hack, K.J., and Riehl, J.P., "Trajectory Development and Optimization of an RBCC-based Launch Vehicle," AAS 99–347, AAS/AIAA Astrodynamics Specialist Conference, Girdwood, AK, 16–19 August, 1999.

[2] Yungster, S., and Trefny, C.J., "Analysis of a New Rocket-Based Combined-Cycle Engine Concept at Low Speed," AIAA 99–2393, 35th AIAA/ASME/SAE/ASEE Joint Propulsion Conference and Exhibit, June 20–24, 1999.

[3] Trefny, C.J. "An Airbreathing Launch Vehicle Concept for Single Stage to Orbit," AIAA 99–2730, 35th AIAA/ASME/SAE/ASEE Joint Propulsion Conference and Exhibit, 20-23 June, 1999

[4] Thomas, S.R., Palac, D.T., Trefny, C.J., and Roche, J.M., "Performance Evaluation of the NASA GTX RBCC Flowpath," NASA/TM—2001-210953.

[5] DeLoach, R. "Applications of Modern Experiment Design to Wind Tunnel Testing at NASA Langley Research Center," AIAA paper 98–0713, January 1998.

[6] Myers, R.H., Khuri, A.I., and Carter, W.H., Jr., "Response Surface Methodology: 1966–1988," *Technometrics*, vol. 31, no. 2, May 1989.

[7] Murman, E.M., Walton, M., and Rebentisch, E., "Challenges in the better, faster, cheaper era of aeronautical design, engineering, and manufacturing," *Aeronautical Journal*, 104: (1040) pp. 481–89, October 2000.

[8] Greitzer, E.M., and Wisler, D.C., "Gas Turbine Compressor Technology: Status and Opportunities," Proceedings of the International Gas Turbine Congress 1999 Kobe, Japan, November 14–19, pp. 39–47.

[9] Frenklach, M., "Modeling," Chapter 7 of Combustion Chemistry, Gardiner, W.C. Jr., Editor, Springer-Verlag, New York, NY, 1984.

[10] Frenklach , M., Wang, H., and Rabinowitz, M.J., "Optimization and Analysis of Large Chemical Kinetic Mechanisms Using the Solution Mapping Method—Combustion of Methane," *Prog. Energy Combust. Sci.*, 1992, Vol. 18, pp. 47–73.

[11] Giunta, A.A., Balabanov, V., Haim, D., Grossman, B., Mason, W.H., Watson, L.T., and Haftka, R.T., "Multidisciplinary Optimisation of a Supersonic Transport Using Design of Experiments Theory and Response Surface Modelling," *The Aeronautical J.*, paper no. 2260, October 1997.

[12] Tolle, R., "A New Optimum Design Code for Hypersonic Nozzles, Utilizing Response Surface Methodology," AIAA Paper, 97–0519, 1997.

[13] Steffen, C.J., Jr., Smith, T.D., Yungster, S., and Keller, D.J., "Computational Analysis for Rocket-Based Combined-Cycle Systems During All-Rocket Mode," *AIAA Journal of Propulsion and Power*, Vol. 16, No. 6, pp. 1030–1039, Nov-Dec 2000.

[14] Madsen, J.I., Shyy, W., and Haftka, R.T., "Response Surface Techniques for Diffuser Shape Optimization," *AIAA Journal*, Vol. 38, No. 9, pp. 1512–18, September 2000.

[15] Papila, M. and Haftka, R.T., "Response Surface Approximations: Noise, Error Repair, and Modeling Errors," *AIAA Journal*, Vol. 38, No. 12, December 2000.

[16] Sacks, J., Welch, W.J., Mitchell, T.J., and Wynn, H.P., "Design and Analysis of Computer Experiments," *Statistical Science*, Vol. 4, No. 4, pp. 409–35, 1989.

[17] Sacks, J., Schiller, S.B., and Welch, W.J., "Designs for Computer Experiments," *Technometrics*, Vol. 31, No. 1, February 1989.

[18] Booker, A.J., "Design and Analysis of Computer Experiments," AIAA paper 98–4757.

[19] Rutherford, B., "An Algorithmic Approach to Experimental Design for the Computer Analysis of a Complex System," Sandia National Laboratories Report, SAND2000-0871, April 2000.

[20] Sasena, M.J., "Optimization of Computer Simulations via Smoothing Splines and Kriging Metamodels," Master Degree Thesis, Univ. of Michigan, Department of Mechanical Engineering, Ann Arbor, MI, 1998

[21] Giunta, A.A. and Watson, L.T., "A Comparison of Approximation Modeling Techniques: Polynomial Versus Interpolating Models," AIAA paper 98–4758.

[22] Simpson, T.W., Korte, J.J., Mauery, T.M., and Mistree, F., "Comparison of Response Surface and Kriging Models for Multidisciplinary Design Optimization," AIAA paper 98–4755.

[23] DeBonis, J.R., Trefny, C.J. and Steffen, C.J., Jr., "Inlet Development for a Rocket Based Combined Cycle, Single Stage to Orbit Vehicle Using Computational Fluid Dynamics," AIAA 99–2239, 35th AIAA/ASME/SAE/ASEE Joint Propulsion Conference and Exhibit, June 2024, 1999.

[24] Steffen, C.J., Jr., and DeBonis, J.R., "Numerical Analysis of the Trailblazer Inlet Flowfield for Hypersonic Mach Numbers," AIAA Paper 2000-0889.

[25] DeBonis, J.R., Trefny, C.J., "Supersonic Wind Tunnel Tests of a Half-Axisymmetric, 12-degree Spike Inlet to an RBCC Propulsion System," paper presented at 2000 JANNAF Joint Subcommittee Meetings, Monterey, CA, November 2000.

[26] Kim, H.D., and Frate, F.C., Experimental Evaluation of the Effect of Angle-of-Attack on Mass Capture of a Symmetric Three-Engine Air Breathing Launch Vehicle Configuration at Supersonic Speeds," paper presented at 2000 JANNAF Joint Subcommittee Meetings, Monterey, CA, November 2000. (NASA/TM—2001-210565)
[27] Frate, F.C., and Kim, H.D., "Wind Code Application to External Forebody Flowfields with Comparisons to Experimental Results," AIAA paper 2001–0226.
[28] GASP Version 3, User's Manual, ISBN 0-9652780-0-X, AeroSoft, Inc., 1996, Blacksburg, VA
[29] Gordon, S. and McBride, B.J., "Computer Program for Calculation of Complex Chemical Equilibrium Compositions and Applications; Part I, Analysis," NASA Reference Publication 1311, October 1994, Cleveland, OH.
[30] Design Expert 6, Users' Manual, Stat-Ease, Inc., Minneapolis, MN.
[31] CRC Standard Mathematical Tables, 28th edition, Beyer, W.H., Editor, CRC Press, Boca Raton, FL, 1987.
[32] Heiser, W.H., and Pratt, D.T., Hypersonic Airbreathing Propulsion, AIAA Education Series, J.S. Przemieniecki, Series Editor-in-Chief, ISBN 1-56347-035-7, 1994.
[33] Steffen, C.J. Jr., and Yungster, S., Computational Analysis of the Combustion processes in an Axisymmetric, RBCC Flowpath," NASA/TM 2001-210679.
[34] Povinelli, F.P., and Povinelli, L.A., "Correlation of secondary sonic and supersonic gaseous jet penetration into supersonic crossflow," NASA TN D-6370, June, 1971.
[35] Baurle, R.A., Fuller, R.P., White, J.A., Chen, T.H., Gruber, M.R., and Nejad, A.S., "An Investigation of Advanced Fuel Injection Schemes for Scramjet Combustion," AIAA paper 98–0937.
[36] GASP Version 4, User's Manual, ISBN 0-9652780-5-0, AeroSoft, Inc., 2001, Blacksburg, VA.
[37] Wilcox, D.C., Turbulence Modeling for CFD, second edition, DCW Industries, Inc, La Canada, CA, July, 1998 (see page 122 of the second printing for a description of the 1998 version of the k-ω model).
[38] Roache, P.J., "Perspective: A Method for Uniform Reporting of Grid Refinement Studies," *Journal of Fluids Engineering*, Vol. 116, 1994.
[39] Hirsch, C., Numerical Computation of Internal and External Flows, Vol. 1: Fundamentals of Numerical Discretization, John Wiley and Sons, 1988, ISBN 0 471 92385 0 (see pages 325–329).
[40] Wolfram, Stephen, The Mathematica Book, 3rd ed., (Wolfram Media/Cambridge University Press, 1996).
[41] "Guide for the Verification and Validation of Computational Fluid Dynamics Simulations," AIAA guide G-077-1998
[42] Shih, T. I-P., Gu, X., and Chu, D., "Grid-Quality Measures and Error Estimates," pp. 799–808, Numerical Grid Generation in Computational Field Simulations, Soni, B.K., and Thompson, J.F., and Hauser, J., and Eiseman, P.R., Editors, International Society of Grid Generation, Mississippi State University, 2000.
[43] Oberkampf, W.L., DeLand, S.M., Rutherford, B.M., Diegert, K.V., and Alvin, K.F., "Estimation of Total Uncertainty in Modeling and Simulation," Sandia National Laboratories Report SAND2000-0824, April 2000.
[44] Deming, W.E., Out of the Crisis, MIT Press, ISBN 0-262-54115-7, August 2000 (paperback edition).

REPORT DOCUMENTATION PAGE

Form Approved
OMB No. 0704-0188

1. AGENCY USE ONLY (Leave blank)	2. REPORT DATE	3. REPORT TYPE AND DATES COVERED
	March 2002	Technical Memorandum

4. TITLE AND SUBTITLE

Response Surface Modeling of Combined-Cycle Propulsion Components Using Computational Fluid Dynamics

5. FUNDING NUMBERS

WU–708–90–63–00

6. AUTHOR(S)

C.J. Steffen, Jr.

7. PERFORMING ORGANIZATION NAME(S) AND ADDRESS(ES)

National Aeronautics and Space Administration
John H. Glenn Research Center at Lewis Field
Cleveland, Ohio 44135–3191

8. PERFORMING ORGANIZATION REPORT NUMBER

E–13204

9. SPONSORING/MONITORING AGENCY NAME(S) AND ADDRESS(ES)

National Aeronautics and Space Administration
Washington, DC 20546–0001

10. SPONSORING/MONITORING AGENCY REPORT NUMBER

NASA TM—2002-211379
AIAA–2002–0542

11. SUPPLEMENTARY NOTES

Prepared for the 40th Aerospace Sciences Meeting and Exhibit sponsored by the American Institute of Aeronautics and Astronautics, Reno, Nevada, January 14–17, 2002 (Invited). Responsible person, C.J. Steffen, Jr., organization code 5880, 216–433–8508.

12a. DISTRIBUTION/AVAILABILITY STATEMENT

Unclassified - Unlimited
Subject Categories: 34, 64 and 66 Distribution: Nonstandard

Available electronically at http://gltrs.grc.nasa.gov/GLTRS

This publication is available from the NASA Center for AeroSpace Information, 301–621–0390.

12b. DISTRIBUTION CODE

13. ABSTRACT (Maximum 200 words)

Three examples of response surface modeling with CFD are presented for combined cycle propulsion components. The examples include a mixed-compression-inlet during hypersonic flight, a hydrogen-fueled scramjet combustor during hypersonic flight, and a ducted-rocket nozzle during all-rocket flight. Three different experimental strategies were examined, including full factorial, fractionated central-composite, and D-optimal with embedded Plackett-Burman designs. The response variables have been confined to integral data extracted from multidimensional CFD results. Careful attention to uncertainty assessment and modeling bias has been addressed. The importance of automating experimental setup and effectively communicating statistical results are emphasized.

14. SUBJECT TERMS

Aeronautics; Fluid mechanics; Heat transfer; Numerical analysis; Systems analysis; Quality assurance; Reliability

15. NUMBER OF PAGES

24

16. PRICE CODE

17. SECURITY CLASSIFICATION OF REPORT	18. SECURITY CLASSIFICATION OF THIS PAGE	19. SECURITY CLASSIFICATION OF ABSTRACT	20. LIMITATION OF ABSTRACT
Unclassified	Unclassified	Unclassified	